Spin–Orbit and Vibronic Coupling in the Ionic Ground State of Iodoacetylene from a Rotationally Resolved Photoelectron Spectrum

Author(s):
Gans, Bérenger; Grassi, Guido; Merkt, Frédéric

Publication date:
2013-10-03

Permanent link:
https://doi.org/10.3929/ethz-a-010780388

Originally published in:
The Journal of Physical Chemistry A 117(39), https://doi.org/10.1021/jp310241d

Funding acknowledgement:
135342 - Rydberg states, VUV laser spectroscopy and photoionization dynamics (SNF)

The following article appeared in *J. Phys. Chem. A* **117**, 9353-9362 (2013) and may be found at http://dx.doi.org/10.1021/jp310241d.

Spin-Orbit and Vibronic Coupling in the Ionic Ground State of Iodoacetylene from a Rotationally Resolved Photoelectron Spectrum

Bérenger Gans, Guido Grassi, and Frédéric Merkt*

Laboratorium für Physikalische Chemie, ETH Zürich, CH-8093 Zürich, Switzerland

E-mail: frederic.merkt@phys.chem.ethz.ch

Phone: +41-44-63 2 43 67. Fax: +41-44-63 2 10 21

*To whom correspondence should be addressed

Keywords: HC_2I, Renner-Teller effect, spin-orbit coupling, PFI-ZEKE photoelectron spectroscopy

Abstract

The $X^+\ ^2\Pi \leftarrow X\ ^1\Sigma^+$ photoionizing transition of iodoacetylene (HC_2I) has been investigated by pulsed-field-ionization zero-kinetic-energy (PFI-ZEKE) photoelectron spectroscopy. The resolution of the rotational structure of the spectra and its analysis provided information on the structure of the HC_2I^+ cation and the photoionization dynamics of HC_2I. In the ground electronic $^2\Pi$ state, the HC_2I^+ cation is found to be linear and subject to a strong spin-orbit coupling. The first adiabatic ionization energy of HC_2I and the spin-orbit splitting of the $X^+\ ^2\Pi$ ground state of HC_2I^+ were determined to be $E_I(HC_2I)/hc = 78296.5(2)$ cm^{-1} and $\Delta\tilde{\nu}_{SO} = 3257(1)$ cm^{-1}, respectively. The large spin-orbit splitting almost entirely masks the Renner-Teller effect which is only detectable through the observation of the nominally forbidden transition to the first excited level (5^1) of the HCC-I bending mode ν_5. The splitting of ~ 2 cm^{-1} observed between the 5^1 levels of $^2\Sigma_{1/2}$ and the $^2\Delta_{5/2}$ symmetry is attributed to a vibronic interaction with the B $^2\Sigma^+$ electronic state of HC_2I^+. The spin-orbit energy level structure of tri- and tetra-atomic molecules subject to the Renner-Teller effect and spin-orbit coupling is discussed for the two limiting cases where the spin-orbit-coupling constant is much smaller and much larger than the bending-mode frequencies.

Introduction

Positively charged radical cations of the family HC_2X^+ (X= F, Cl, Br and I) are prototype systems to study the Renner-Teller effect and spin-orbit interactions in open-shell molecules. Several studies of these cations have been carried out by photoelectron spectroscopy,[1,2] emission, and laser-excitation spectroscopy.[3–6]

HC_2I in its ground $X\ ^1\Sigma^+$ electronic state and HC_2I^+ in its ground $^2\Pi$ electronic state are linear molecules possessing five vibrational modes: ν_1 (C-H stretch), ν_2 (C-C stretch), ν_3 (C-I stretch), ν_4 (C-C-H bend) and ν_5 (C-C-I bend). The first three modes (ν_1, ν_2 and ν_3) have Σ^+ symmetry and

the remaining two (ν_4 and ν_5) have Π symmetry. These latter two modes are Renner-Teller-active modes in the ground electronic state of the HC_2I^+ cation.

The $X^+\ ^2\Pi$ ground electronic state of HC_2I^+ is formed by ejecting an electron out of one of the p_π orbitals centered on the iodine atom. A strong spin-orbit interaction results which splits the ground state into its $^2\Pi_{3/2}$ and $^2\Pi_{1/2}$ components by $\sim$ 0.4 eV. The spin-orbit splitting in the ground state of HC_2I^+ is therefore much larger than the fundamental vibrational energies of the Renner-Teller active modes, so that the overall spin-vibronic coupling situation differs from that usually encountered in other molecules subject to both the Renner-Teller effect and spin-orbit coupling. This difference is illustrated qualitatively by the correlation diagram depicted in panel b) of Fig. 1, in which the left-hand side corresponds to the "usual" situation for which the spin-orbit splitting is comparable or smaller than the vibrational spacings (adapted from Fig. 8 of Ref. 7) and the right-hand side corresponds to the situation encountered in the ground state of HC_2I^+. The two spin-orbit components of the X^+ ground state of HC_2I^+ may therefore be regarded in first approximation as two distinct electronic states with their own vibrational structure.

The Renner-Teller effect can be viewed as a coupling of the orbital and vibrational angular momenta and the spin-orbit coupling as a coupling of the orbital and electron-spin angular momenta. The Renner-Teller effect and the spin-orbit interaction are therefore in competition, and one may expect that the very strong spin-orbit coupling in HC_2I^+ largely quenches the observable effects of the Renner-Teller interaction. For this reason, the Renner-Teller effect was not explicitly considered in the previous high-resolution spectroscopic studies of HC_2I^+.[4,6]

The high-resolution photoelectron spectra of HC_2I presented in this article confirm this qualitative behavior and, in addition, enable the quantification of the hierarchy of interaction strengths encountered in this prototypical radical cation. The emphasis of our study is placed on the analysis of the spin-orbit interaction and on the level structure of the 5^1 level of the $^2\Pi_{3/2}$ state. Our spectroscopic observation of a weak splitting between the $^2\Sigma_{1/2}$ and the $^2\Delta_{5/2}$ components of this 5^1 level is analyzed and discussed within the framework of theoretical models of the Renner-Teller effect in triatomic molecules[8–11] and their extension to linear tetraatomic molecules.[12–15]

Experiment

The PFI-ZEKE photoelectron spectra presented in this study were recorded using two different laser systems. The spectra of the $X^+\,^2\Pi_{3/2}\,(v=0) \leftarrow X\,^1\Sigma^+\,(v=0)$ (referred to as $(0_0^0,\,\Omega=\frac{3}{2})$ band in the following) and the $X^+\,^2\Pi_{3/2}\,(v_5=1) \leftarrow X\,^1\Sigma^+\,(v=0)$ (referred to as $(5_0^1,\,\Omega=\frac{3}{2})$ band) transitions were obtained using a photoelectron spectrometer[16] coupled with a narrow-bandwidth (0.008 cm^{-1}) vacuum-ultraviolet laser source[17] tunable between 78000 and 78500 cm^{-1}. The spectra of the $X^+\,^2\Pi_{1/2}\,(v=0) \leftarrow X\,^1\Sigma^+\,(v=0)$ (referred to as $(0_0^0,\,\Omega=\frac{1}{2})$ band) and the $X^+\,^2\Pi_{3/2}\,(v_1=1) \leftarrow X\,^1\Sigma^+\,(v=0)$ (referred to as $(1_0^1,\,\Omega=\frac{3}{2})$ band) transitions in the range of 81500-82000 cm^{-1} were measured at lower resolution using the tunable VUV laser system described in Ref. 18 (bandwidth 0.3 cm^{-1}), primarily to determine the value of the spin-orbit splitting.

Pulses of VUV radiation were generated using two tunable lasers pumped by the second harmonic (532 nm) of a Nd:YAG laser by difference-frequency mixing ($2\nu_{UV}-\nu_2$) in krypton. The VUV radiation was spatially separated from the fundamental beams of frequencies ν_{UV} and ν_2 using a LiF prism. For the high-resolution experiments, the fundamental beams of frequency ν_{UV} and ν_2 were generated using two pulsed-amplified ring dye lasers resulting in a VUV laser bandwidth of 0.01 cm^{-1}. The measurements at lower resolution were carried out using two commercial pulsed dye lasers. In both cases, the wavenumber $\tilde{\nu}_1$ of the first laser was tripled using two successive BBO crystals and the tripled output $\tilde{\nu}_{UV}=3\tilde{\nu}_1$ was held fixed at the position of the $(4p)^6 \rightarrow (4p)^5 5p[1/2]_0$ two-photon resonance of atomic krypton ($2\tilde{\nu}_{UV}=94092.87 cm^{-1}$). The VUV wavenumber was scanned by tuning the wavenumber $\tilde{\nu}_2$ of the second laser. The absolute calibration of the high-resolution spectra was performed by recording laser-induced-fluorescence spectra of iodine and monitoring the transmission spectrum through several etalons using a small fraction of the output of the second laser (ν_2) and by locking the fundamental frequency of the first laser (ν_1) to a single hyperfine component of the Doppler-free iodine spectrum. This procedure resulted in an absolute accuracy of 0.02 cm^{-1}. The spectra recorded at lower resolution with the second laser system were calibrated at an absolute accuracy of 0.5 cm^{-1} by recording the optogalvanic spectrum of Ne while the frequency of the second laser (ν_2) was scanned.

Iodoacetylene was synthesized in two steps. In the first step (see Reaction I in Scheme 1), tributylchlorostannane was reacted with sodium acetylide to tributyl(ethynyl)stannane in diethylether (8h reflux) according to a german patent.[19] In the second step (see Reaction II in Scheme 1), iodoacetylene was formed from tributyl(ethynyl)stannane and I_2 ($T = 0-10$°C, $p = 0.5-2$ mbar) following a method adapted from Ku *et al.*[20] To obtain iodoacetylene in pure form, the reaction of tributyl(ethynyl)stannane with iodine was performed in tetraethyleneglycoldimethylether as a high boiling solvent under vacuum conditions, and the product was condensed in a cooling trap and transferred to a lecture bottle. The synthesis, which combines the advantages of good yield, high purity and the possibility to generate a large HC_2I sample in pure form, is described in more detail in the Supporting Information.

A mixture of $\approx 5\%$ of HC_2I diluted in argon was introduced in the experiment by means of a supersonic beam emitted by a 25 Hz pulsed valve (General Valve) with reservoir held at a stagnation pressure of 1-1.5 bar. After traversing a skimmer (diameter 0.5 mm), the cold molecular beam crossed the VUV laser at right angles in the photoexcitation region. In the supersonic beam, the population of rotational levels in the X $^1\Sigma^+$ ground state of HC_2I approximately corresponded to a thermal distribution at $T_{\rm rot} = 5$ K. No significant population of excited vibrational levels could be detected.

Pulsed-field-ionization zero-kinetic-energy (PFI-ZEKE) photoelectron spectra[21] of HC_2I were recorded by monitoring the electrons produced by pulsed-field-ionization of the long-lived high Rydberg states located below the successive ionization thresholds as a function of the VUV wavenumber. To achieve a high-resolution, multipulse electric-field sequences were employed as described in Ref. 16. Theses pulse sequences consisted of a positive discrimination field pulse of 166 mV/cm and 1 μs duration, followed immediately by successive 200-ns-long negative pulses (-83 / -116 / -149 / -183 / -216 / -249 / -299 / -332 / -415 / -830 mV/cm for the $(0_0^0, \Omega = \frac{3}{2})$ band, -83 / -166 / -249 / -830 mV/cm for the $(5_0^1, \Omega = \frac{3}{2})$ band and -166 / -830 mV/cm for the $(0_0^0, \Omega = \frac{1}{2})$ and $(1_0^1, \Omega = \frac{3}{2})$ bands). The electron signals produced by each of these negative electric fields were integrated and recorded separately as a function of the laser wavenumber. The

field-induced shift of the ionization thresholds were corrected following the procedure described in Ref. 16. In order to increase the signal-to-noise ratio, the spectra obtained with different negative pulses were added after correction of the field-induced shifts. Spectral resolutions of 0.17 cm^{-1} and 0.3 cm^{-1} resulted for the spectra of the $(0_0^0, \Omega = \frac{3}{2})$ and $(5_0^1, \Omega = \frac{3}{2})$ bands respectively. Spectra of the $(0_0^0, \Omega = \frac{1}{2})$ and $(1_0^1, \Omega = \frac{3}{2})$ bands were recorded at a resolution of 1 cm^{-1}.

Renner-Teller effect and spin-orbit coupling

The Renner-Teller effect and spin-orbit coupling in triatomic molecules.

In a molecule subject to the Renner-Teller effect, one needs to consider the vibrational angular momentum associated with the degenerate vibrational modes in addition to the electronic orbital and spin angular momenta. In a linear molecule with N atoms, there are $N-2$ degenerate modes of Π symmetry, each of which contributes $\hbar l_i$ ($l_i = -v_i, -v_i+2, ..., v_i$; v_i represents the vibrational quantum number of the degenerate mode i) to the projection of the total vibrational angular momentum ($\hbar l = \hbar \sum_i l_i$) along the symmetry axis.[7] In the absence of spin, the projection of the total angular momentum onto the symmetry axis is $\hbar K = \hbar(\Lambda + l)$ where Λ is the quantum number associated with the projection of the orbital angular momentum. Here, Λ is defined as a signed quantity, *i.e.*, $\Lambda = \pm 1$ for a Π electronic state. In molecules with a nonzero total electron spin $\vec{S}$ following a Hund's-case-(a)-type angular-momentum-coupling scheme, the quantum number P associated with the projection of the total vibronic angular momentum on the symmetry axis is given by $P = \Lambda + \Sigma + l$. According to common practice,[7] the vibronic levels are labeled ${}^{2S+1}|K|_{|P|}$.

Neglecting the effects of spin, the electronic state is degenerate in the linear configuration. The Renner-Teller effect leads to a removal of the degeneracy when the molecule bends along mode i and the splitting between the two potential curves can be determined using Eq. (1)

$$V^+ - V^- = \left(\frac{1}{2}k^+ r^2 + k_4^+ r^4 + ...\right) - \left(\frac{1}{2}k^- r^2 + k_4^- r^4 + ...\right), \quad (1)$$

where V^+ and V^- are the potential energy functions, $k^{+/-}$ and $k_4^{+/-}$ the quadratic and quartic force constants, respectively, and r the bending coordinate.[7] The values of k^+ and k^- determine the Renner-Teller coupling parameter

$$\varepsilon = \frac{k^+ - k^-}{k^+ + k^-}. \tag{2}$$

The correlation diagram of vibronic energy levels presented in Fig. 1a describes the situation encountered in the $^2\Pi$ state of a triatomic molecule of $C_{\infty v}$ point-group symmetry for $A \ll \omega_b$ (where A is the spin-orbit constant and ω_b the harmonic wavenumber of the bending mode), which is the most common situation.[7,22] On the left-hand side of Fig. 1a, the Renner-Teller effect is assumed to be vanishing ($\varepsilon = 0$), and the energy-level structure consists of pairs of levels separated by the spin-orbit-coupling constant A. On the right-hand side, the spin-orbit-coupling constant is assumed to be zero, and the Renner-Teller effect splits the first excited vibrational level into three components. The combined effect of the spin-orbit and Renner-Teller interactions splits each vibrational level v_b into $2(v_b+1)$ components and leads to the situation depicted in the middle of Fig. 1a. The lower panel of Fig. 1 illustrates schematically how the energy-level structure evolves when A increases and becomes much larger than ω_b, which is the situation encountered in the X $^2\Pi$ ground state of HC_2I^+ when only one Renner-Teller active mode is considered.

The energy level structure of a triatomic molecule which is subject to the Renner-Teller and spin-orbit coupling can be calculated by determining the eigenvalues of the effective Hamiltonian $H_{eff} = H_{vib} + H_{SO} + H_{RT}$ consisting of contributions from the vibrational motion (H_{vib}), the spin-orbit coupling (H_{SO}) and the Renner-Teller effect (H_{RT}).[22]

The diagonal matrix elements of H_{eff} are

$$\langle \Lambda = \pm 1, \Sigma = \pm\frac{1}{2}, v_b | H_{vib} + H_{SO} | \Lambda = \pm 1, \Sigma = \pm\frac{1}{2}, v_b, \rangle = \omega_b(v_b+1) + A_{eff}\Lambda\Sigma, \tag{3}$$

where

$$A_{\text{eff}} = A[1 - \frac{g_K}{\omega_{\text{b}}}(v_{\text{b}} + 1)] \tag{4}$$

is an effective spin-orbit-coupling constant which includes the effect of the interaction with the neighboring $^2\Sigma$ and $^2\Delta$ electronic states[9,10] (see also later in this section).

The off-diagonal matrix elements of H_{eff} obeying the selection rule $\Delta v_{\text{b}} = 0$ and $\Delta l_{\text{b}} = -\Delta\Lambda = 2$ ($\Delta K = 0$) can be evaluated with Eq. (5)

$$\langle \Lambda = 1, v_{\text{b}}, l_{\text{b}} | \text{H}_{\text{RT}} | \Lambda = -1, v_{\text{b}}, l_{\text{b}} + 2 \rangle = \frac{1}{2} \varepsilon_{\text{b}} \omega_{\text{b}} \left[(v_{\text{b}} + 1)^2 - K^2 \right]^{1/2} \tag{5}$$

and those obeying the selection rule $\Delta v_{\text{b}} = \pm 2$ and $\Delta l_{\text{b}} = -\Delta\Lambda = 2$ ($\Delta K = 0$) with Eq. (6)

$$\langle \Lambda = 1, v_{\text{b}}, l_{\text{b}} | \text{H}_{\text{RT}} | \Lambda = -1, v_{\text{b}} \pm 2, l_{\text{b}} + 2 \rangle = \frac{1}{4} \varepsilon_{\text{b}} \omega_{\text{b}} \left[(v_{\text{b}} \pm K \pm 1)(v_{\text{b}} + 2 \pm K \pm 1) \right]^{1/2}. \tag{6}$$

In Eqs. (5) and (6), ε_{b} represents the Renner-Teller coupling parameter as defined in Eq. (2).

The following additional phenomena can also affect the energy-level structure of $^2\Pi$ states of triatomic molecules subject to the Renner-Teller effect:

1. Fermi interactions,[8,23,24] which couple bending and stretching levels of the same vibrational symmetry and can lead to strong perturbations when the wavenumber of one of the stretching vibrations is approximately twice as large as the wavenumber of the bending vibration.

2. Sears resonances,[23,25,26] which couple bending levels v_{b} of the lower spin-orbit component ($^2\Pi_{3/2}$ for an inverted system) with $v_{\text{b}} - 1$ levels of the upper spin-orbit component ($^2\Pi_{1/2}$) according to the selection rules $\Delta K = \pm 1$, $\Delta\Sigma = \mp 1$ and $\Delta P = 0$. The resonances are observable whenever the bending wavenumber closely matches the spin-orbit splitting and can be regarded as being mediated by vibronic interactions involving $^2\Sigma$ or $^2\Delta$ electronic states.[23,25] They can also be described as a purely relativistic effect.[26]

3. vibronic interactions with $^2\Sigma$ or $^2\Delta$ electronic states which shift the position of the $^2\Delta$ vibronic component of the $v_5 = 1$ level relative to that of the $^2\Sigma$ component.[9] The effect of these interactions can be taken into account by including the contribution

$$g_K \Lambda (\Lambda + l_\mathrm{b}) = g_K \Lambda K \tag{7}$$

to the diagonal elements of H_{eff}. The magnitude of g_K decreases with the energy difference between the $^2\Pi$ and the $^2\Sigma$ or $^2\Delta$ electronic states. Higher-order anharmonic terms have been derived by Gauyacq and Jungen.[10] The contributions from these terms increase with the bending vibrational quantum number. At our resolution, we do not expect them to be observable in a spectrum of the fundamental of the bending mode v_5 and therefore we shall not consider them further.

In cases where the spin-orbit-coupling constant is very large, one expects a significant mixing of the $^2\Pi_{1/2}$ component of the ground state with higher-lying $^2\Sigma_{1/2}$ states, as for instance in Xe_2^+.[27] The $^2\Pi_{3/2}$ ground-state component, however, is not affected because it has $\Omega = \frac{3}{2}$. The $^2\Pi_{1/2}$ - $^2\Sigma_{1/2}$ mixing induced by the spin-orbit interaction is likely to be the main reason for the differences in the vibrational spacings observed experimentally for the two spin-orbit components of Renner-Teller-active molecules subject to strong spin-orbit coupling such as ICN^+.[28]

To quantify the effects of the competition between the Renner-Teller effect and the spin-orbit coupling, Eqs. (3)-(7) were used to calculate the spin-vibronic energy-level structure for fixed values of the parameters ε_b (0.1), g_K (1 cm^{-1}) and ω_b (234 cm^{-1}) and increasing value of the spin-orbit-coupling constant A_{eff}. The results are depicted in Fig. 2. Fig. 2a shows how the difference between the calculated spin-orbit splitting $\Delta\tilde{\nu}_{\mathrm{SO}}$ and the spin-orbit-coupling constant A_{eff} evolves as the value of A_{eff} changes from 0 (right-hand side) to -3500 cm^{-1} (left-hand side) for the $^2\Pi$ ground state (grey triangles and full line), and for the $^2\Sigma$ (open circles and dotted line) and $^2\Delta$ (full circles and full line) components of the $v_\mathrm{b} = 1$ vibrational level. The dash-dotted line indicates the zero value that is expected in the absence of the Renner-Teller effect. Fig. 2b illustrates how

the origins of the $^2\Sigma$ component (open circles and dotted line) and the $^2\Delta$ component (full circles and full line) of the 5^1 level evolve as $A_{\rm eff}$ increases. The open circles, full circles and triangles correspond to calculations which consider Eqs. (3)-(7), whereas the full and dotted lines in Fig. 2b were obtained in calculations neglecting the vibronic correction given by Eq. (7). From this panel, one sees immediately that this vibronic correction does not affect the $^2\Sigma_{1/2}$ state but shifts the $^2\Delta_{5/2}$ state by $2g_K$, as expected for a $\Lambda = 1,\ K = 2$ level.

Three situations can be distinguished, corresponding to $|A_{\rm eff}| \ll \omega_{\rm b}$, $|A_{\rm eff}| \approx 2\omega_{\rm b}$ and $|A_{\rm eff}| \gg \omega_{\rm b}$. When $|A_{\rm eff}| \gg \omega_{\rm b}$, the splitting between the two spin-orbit components of all three states ($^2\Pi$, $^2\Sigma(v_{\rm b} = 1)$ and $^2\Delta(v_{\rm b} = 1)$) exactly matches the value of the spin-orbit-coupling constant, and the $^2\Sigma_{1/2}$ and $^2\Delta_{5/2}$ components of the $(v_{\rm b} = 1)$ level are split by $2g_K$. In this limiting case, the Renner-Teller effect is not observable and, in particular, does not quench the spin-orbit interaction.

When $|A_{\rm eff}| \ll \omega_{\rm b}$, the spin-orbit splitting $\Delta\tilde{\nu}_{\rm SO}$ of the $^2\Pi$ and the $^2\Delta$ states deviates from $A_{\rm eff}$ and can be described by the formula

$$\Delta\tilde{\nu}_{\rm SO} = A_{\rm eff}\left[1 - \frac{\varepsilon_{\rm b}^2}{16}\left((v_{\rm b}+1)^2 + K(K+2\Lambda)\right)\right] \tag{8}$$

derived by Hougen[8] and extended by Brown[9] and Gauyacq and Jungen[10] to include the vibronic correction for $g_K \neq 0$ (see Eq. (4)). The term in the square bracket in Eq. (8) reduces the value of $\Delta\tilde{\nu}_{\rm SO}$ compared to $A_{\rm eff}$ for the $^2\Pi$ and $^2\Delta(v_{\rm b} = 1)$ states and completely removes the near-degeneracy between the $^2\Sigma_{1/2}$ and $^2\Delta_{5/2}$ states. The energy of the lower (upper) $^2\Sigma$ states is lowered (raised) by the Renner-Teller effect, so that the splitting between the two $^2\Sigma$ states at low values of $A_{\rm eff}$ is entirely of vibronic (and not spin-orbit) origin (see also Fig. 1a).

When $|A_{\rm eff}| \approx 2\omega_{\rm b}$, the $v_{\rm b}$ level of the lower spin-orbit component ($^2\Pi_{3/2}$) becomes degenerate with the $v_{\rm b} - 2$ level of the upper component. The strong resonance effect observed in panel a) at $A_{\rm eff} \approx 2\omega_{\rm b} = 468$ cm^{-1} is caused by the nonzero off-diagonal elements (Eq. (6)) coupling the $^2\Pi_{1/2}$ $(v_{\rm b})$ and the $^2\Pi_{3/2}$ $(v_{\rm b}+2)$ levels.

Generalization to tetraatomic molecules and application to the HC_2I^+ ground state.

The treatment presented above for triatomic molecules can be extended to tetraatomic molecules, which have two Renner-Teller active modes v_4 and v_5.[12–14] He and Clouthier[14] have derived a full effective Hamiltonian for tetraatomic molecules including the interactions $1.-3.$ listed above. The 5^1 bending level of HC_2I^+ lies more than 300 cm^{-1} below all other vibrational levels;[6] moreover, its π symmetry protects it from Fermi interactions. Consequently, we have neglected Fermi interactions in our treatment. The fundamental wavenumber of the v_5 mode ($\omega_5 \approx 234$ cm^{-1}) is much smaller than the spin-orbit-coupling constant ($A > 3250$ cm^{-1}, see below) so that the effects of Sears resonances are negligible. Therefore only interaction 3 needs to be retained to calculate the level structure of HC_2I^+ at low energies.

Following the treatment presented in Ref. 14, we have adapted Eqs. (3)-(7) to the case of the HC_2I^+ $X^+\,{}^2\Pi$ ground state by

1. replacing $\omega_b(v_b+1)$ in Eq. (3) by $\omega_4(v_4+1)+\omega_5(v_5+1)$;

2. generalizing the expressions of the off-diagonal elements to include both Renner-Teller active modes and their coupling. Instead of only one Renner-Teller parameter (ε_b), three parameters are needed, one for each mode (ε_4 and ε_5) and one for their anharmonic coupling (ε_{45}), so that Eqs. (5) and (6) must be applied to both modes (v_4 and v_5) and the additional off-diagonal element given by Eqs. (9) and (10) must be included

   - $\Delta(v_i+v_j)=0$ ($i=4,5$ and $j=5,4$):

$$\begin{aligned}\langle \Lambda=1,v_i,l_i,v_j,l_j|\mathrm{H_{RT}}|\Lambda=-1,v_i+1,l_i+1,v_j-1,l_j+1\rangle \\ = \tfrac{1}{4}\varepsilon_{45}(\omega_4\omega_5)^{1/2}\left[(v_i+l_i+2)(v_j-l_j)\right]^{1/2}\end{aligned} \tag{9}$$

- $\Delta(v_i + v_j) = \pm 2$ ($i = 4,5$ and $j = 5,4$):

$$\begin{aligned}\langle \Lambda = 1, v_i, l_i, v_j, l_j | \mathrm{H_{RT}} | \Lambda = -1, v_i \pm 1, l_i + 1, v_j \pm 1, l_j + 1 \rangle \\ = \tfrac{1}{4}\varepsilon_{45}(\omega_4\omega_5)^{1/2}\left[(v_i \pm l_i + \tfrac{2}{0})(v_j \pm l_j + \tfrac{2}{0})\right]^{1/2}\end{aligned} \tag{10}$$

3. adding a second term to the expression (7) describing the coupling to other $^2\Sigma$ or $^2\Delta$ electronic states, which now becomes:[14]

$$g_K(4)\Lambda(\Lambda + l_4) + g_K(5)\Lambda(\Lambda + l_5) \tag{11}$$

The effect of the spin-orbit-coupling constant on the vibronic structure is similar to the triatomic case described above. When $|A| \ll (\omega_4, \omega_5)$, we find that the spin-orbit splittings of the $^2\Pi$, 5^1 and 4^1 $^2\Delta$ states, and 5^2 and 4^2 $^2\Phi$ states are well approximated by

$$\begin{aligned}\Delta\tilde{\nu}_{\mathrm{SO}} = A_{\mathrm{eff}} \quad \times \quad & \left[1 - \frac{1}{16}\varepsilon_4^2\left((v_4+1)^2 + K(3\Lambda + l_4)\right)\right. \\ & -\frac{1}{16}\varepsilon_5^2\left((v_5+1)^2 + K(3\Lambda + l_5)\right) \\ & \left.-\frac{1}{8}\varepsilon_{45}^2\frac{\omega_4\omega_5}{(\omega_4+\omega_5)^2}(v_4 + l_4 + 2)(v_5 + l_5 + 2)\right],\end{aligned} \tag{12}$$

[where $A_{\mathrm{eff}} = A\left(1 - \frac{g_K(4)}{\omega_4}(v_4+1) - \frac{g_K(5)}{\omega_5}(v_5+1)\right)$] and now depend on ε_4, ε_5, ε_{45}, $g_K(4)$ and $g_K(5)$. Eq. (12) is an extension of the formulae derived for triatomic molecules by Gauyacq and Jungen[10] and for tetraatomic molecules by Tang and Saito.[12] It differs from the expression derived by Tang and Saito who have neglected the vibronic correction (i.e., $g_K(4) = g_K(5) = 0$) and obtained a slightly different dependence on K and Λ. When $|A_{\mathrm{eff}}| \approx (\omega_4, \omega_5)$, three resonances occur when $|A_{\mathrm{eff}}| \approx 2\omega_4$, $|A_{\mathrm{eff}}| \approx 2\omega_5$ and $|A_{\mathrm{eff}}| \approx \omega_4 + \omega_5$ and are caused by the nonzero off-diagonal elements (Eqs. (6) and (10)). As in the case of triatomic molecules, the Renner-Teller effect tends to be unobservable when $|A_{\mathrm{eff}}| \gg (\omega_4, \omega_5)$, and the spin-orbit splitting $\Delta\tilde{\nu}_{\mathrm{SO}}$ matches the spin-orbit-coupling constant A_{eff}. The splitting between the $^2\Delta_{5/2}$ ($v_5 = 1$) and $^2\Sigma_{1/2}$ ($v_5 = 1$) vibronic

levels now closely approaches the limiting value

$$\Delta\tilde{\nu}(^2\Delta_{5/2} - {}^2\Sigma_{1/2}) = 2g_K(5) + g_K(4). \tag{13}$$

To model the Renner-Teller effect in HC_2I^+ at low energies, we therefore used Eqs. (9)-(10) and included the effects of the vibronic interaction term given by Eq. (11), because the B $^2\Sigma^+$ is located 5 eV above the $^2\Pi_{3/2}$ ground state and previous investigations have revealed measurable effects in cases where the interacting electronic states are located $\sim$ 5 eV apart. In CO_2^+, for instance, the A $^2\Sigma_u^+$ is located 4.5 eV above the X $^2\Pi_g$ ground state and gives rise to a value of g_K of about 3 cm^{-1}.[10,11] We also chose to neglect the anharmonicity corrections to the vibronic interaction with the distant $^2\Sigma$ and $^2\Delta$ states which give rise to the terms involving g_{22},[10] in part because we do not expect such terms to be strong in low vibrational levels, and in part because, even if such terms did make a contribution to the observed splittings, they could not have been extracted from a measurement of the $v_5 = 1$ level.

The large spin-orbit interaction in HC_2I^+ ($\Delta\tilde{\nu}_{SO} = 3257$ cm^{-1}) and the small values of ω_5 (≈ 234 cm^{-1}) and ε_5 correspond to the limiting case $|A| \gg (\omega_4, \omega_5)$ discussed above, which implies that the spin-orbit splitting $\Delta\tilde{\nu}_{SO}$ of the observed levels should be close to $A_{\rm eff}$.

The rotational structure of the $^2\Pi_{3/2}$ and $^2\Delta_{5/2}(v_5 = 1)$ levels was assumed to follow the Hund's case (a) expression[8]

$$E_{\rm rot}(J)/(hc) = B_{v_5}^+ \left[\left(J+\frac{1}{2}\right)^2 - K^2\right] \pm \frac{1}{2}\left[4B_{v_5}^{+2}\left(J+\frac{1}{2}\right)^2 + A_{\rm eff}(A_{\rm eff} - 4KB_{v_5}^+)\right]^{\frac{1}{2}} \tag{14}$$

with $K = 1$ and 2 for the Π and Δ states, respectively and $A_{\rm eff} \approx \Delta\tilde{\nu}_{SO}$ (see Eq. (12)).

For the rotational structure of the $^2\Sigma$ state, we used the Hund's case (c) expression[8]

$$E_{\rm rot}(J)/(hc) = B_{v_5}^+ J(J+1) + \frac{1}{4}B_{v_5}^+ \pm p(J+\frac{1}{2}) \pm \frac{A_{\rm eff}}{2}. \tag{15}$$

with the same value of the rotational constant $B_{v_5}^+$ for the $^2\Delta$ and $^2\Sigma$ components of the 5^1 level and

an Ω-doubling parameter $p = 0$ cm^{-1}, corresponding to the situation $A \gg B$.[7]

Experimental results and discussion

The $(0_0^0, \Omega = 3/2)$ band

The PFI-ZEKE photoelectron spectrum of the $(0_0^0, \Omega = \frac{3}{2})$ origin band of HC_2I is presented in Fig. 3a. At the experimental resolution of ~ 0.15 cm^{-1}, the rotational structure could be partially resolved. The branch structure is characteristic of a $^2\Pi_{3/2} \leftarrow {}^1\Sigma^+$ ionizing transition of a linear molecule and the strong central feature is attributed to the $\Delta J = J^+ - J'' = -1/2$ branch. This branch forms a band head at $J'' \approx 10$, which indicates that the $X^+\ ^2\Pi_{3/2}$ ground state of HC_2I^+ has a larger rotational constant than the $X\ ^1\Sigma^+$ ground state of HC_2I. The intensity distribution of the spectrum is dominated by the two rotational branches with $\Delta J = \pm 1/2$ with weaker contributions from $\Delta J = \pm 3/2$, $\pm 5/2$, $\pm 7/2$ and $\pm 9/2$ branches.

To analyze the rotational structure of the PFI-ZEKE photoelectron spectrum we used Eq. (14) for the rotational levels of the ion and the standard expression

$$E_{\rm rot}(^1\Sigma^+)/(hc) = B_0 J(J+1) - D_0 J^2(J+1)^2 + H_0 J^3(J+1)^3 \qquad (16)$$

for the rotational levels of the neutral, for which precise rotational and centrifugal distortion constants have been determined by Ahonen *et al.*[29] ($B_0 = 0.1059420941(29)$ cm^{-1}, $D_0 \times 10^8 = 1.73392(16)$ cm^{-1} and $H_0 \times 10^{15} = -2.28(10)$ cm^{-1}). Values of $E_{\rm I}/(hc) = 78296.5(2)$ cm^{-1} and $B_0^+ = 0.1093(8)$ cm^{-1} were determined for the adiabatic ionization energy of HC_2I and the ground-state rotational constant of HC_2I^+, respectively, from the observed spectral positions in a least-squares fit. These values are in good agreement with the values $E_{\rm I}(HC_2I) = 9.71(1)$ eV (78320(80) cm^{-1}) obtained earlier by He I photoelectron spectroscopy[1] and the rotational constant $B_0^+ = 0.10959(7)$ cm^{-1} determined by laser excitation spectroscopy.[4]

When modeling the rotational intensity distribution, we obtained good agreement with the

experimental spectrum by assuming that the population of ground rotational levels in the supersonic expansion corresponds to a thermal distribution at 4.5 K, and by weighing the relative intensities of the $\Delta J = \pm 1/2$, $\pm 3/2$, $\pm 5/2$, $\pm 7/2$ and $\pm 9/2$ branches with the factors 1, 0.75, 0.5, 0.3 and 0.1, respectively. Because the angular-momentum conservation rule[30] requires that $|\Delta J_{\max}| = l_{\max} + 3/2$, we conclude that photoelectron partial waves up to $l_{\max} = 3$ contribute to the photoionization cross section, which, in turn, indicates that the orbital from which the photoelectron is ejected has contributions with up to at least $l = 2$. This observation suggests a partial delocalization of the electron hole from the I atom to the C_2H part of the molecule, an aspect we shall return to in the conclusions section.

Panels (c) and (b) of Fig. 3 present the calculated stick spectrum and its convolution with a Gaussian line-shape function with full width at half maximum of 0.17 cm^{-1}, respectively. The agreement between calculated and measured intensities is almost perfect on the high wavenumber side of the strong $\Delta J = -1/2$ branch. On its low wavenumber side, the calculated intensities are a little weaker than the observed ones, an effect that is often observed in PFI-ZEKE photoelectron spectra and results from rotational channel interactions.[31]

The $(5_0^1, \Omega = 3/2)$ band

The PFI-ZEKE photoelectron spectrum of the ν_5 fundamental band of the $(5_0^1, \Omega = \frac{3}{2})$ transition of HC_2I is presented in Fig. 4a. In the absence of the Renner-Teller effect, this transition is forbidden by symmetry, and its intensity is therefore much lower than that of the origin band. Comparison of the relative intensities of these two bands indicates that the 5_0^1 band is at least 20 times weaker than the origin band. The weakness of the 5_0^1 band forced us to apply a less restrictive pulsed-field-ionization sequence, which degraded the spectral resolution to 0.3 cm^{-1}. This lower spectral resolution, combined with the fact that transitions to the two $^2\Sigma_{1/2}$ and $^2\Delta_{5/2}$ vibronic components overlap, made it impossible to resolve individual rotational lines in the PFI-ZEKE photoelectron spectrum. To analyze the spectrum, we therefore attempted to reproduce the four main spectral features of the experimental spectrum centered at 78528.5, 78529, 78529.8 and 78531 cm^{-1}. To

do so, we used Eqs. (14) and (15) to calculate the rotational structure of the $^2\Delta_{5/2}$ and $^2\Sigma_{1/2}$ states, respectively, and Eq. (11) for the splitting between theses two states. We further assumed the same value for the rotational constant (i.e., $B^+_{v_5=1} = B^+_0$) and the same relative intensities of the rotational branches (see previous subsection) as for the origin band, but a reduced ground-state rotational temperature of 2.5 K to account for the higher nozzle stagnation pressure used in the experiment to compensate for the weakness of the 5^1_0 band.

The results of our efforts at modeling the spectrum of the (5^1_0, $\Omega = 3/2$) band are depicted in panels b)-d) of Fig. 4, which present the individual contributions of the $^2\Sigma_{1/2}$ (panel d)) and $^2\Delta_{5/2}$ (panel c)) components and their sum (panel b)). Only three parameters were adjusted in the calculations: (i) the relative intensity of the $^2\Sigma_{1/2}$ and $^2\Delta_{5/2}$ components which we found to be in favor of the latter by a factor of 2; (ii) the position of the origin of the $^2\Delta_{5/2}$ level with respect to the $^2\Pi_{3/2}$ (0^0) ground state, which we determined to be 235 cm^{-1}, and (iii) the splitting $2g_K(5) + g_K(4)$ between the $^2\Delta_{5/2}$ and the $^2\Sigma_{1/2}$ components which amounts to 2.0(2) cm^{-1}.

These results conform to the behavior expected for the $|A| \gg (\omega_4,\ \omega_5)$ limiting case of the Renner-Teller effect in a tetraatomic molecule presented above. The Renner-Teller effect along ν_5 is almost entirely masked by the spin-orbit interaction and only noticeable by the weakly allowed nature of the transition to the 5^1 level. The vibronic interaction with the B $^2\Sigma^+$ electronic state of HC_2I^+ is revealed by the splitting of ~ 2 cm^{-1} between the $^2\Sigma_{1/2}$ and $^2\Delta_{5/2}$ components. Under these conditions, it is not possible to quantify the strength of the Renner-Teller effect in HC_2I^+ from the experimental spectrum more precisely than by stating that ε_4, ε_5 and ε_{45} must all be much smaller than unity given that HC_2I^+ is found to be linear in its electronic ground state.

The (0^0_0, $\Omega = 1/2$) and the (1^1_0, $\Omega = 3/2$) bands

The experimental information available on the $^2\Pi_{1/2}$ spin-orbit component of the $^2\Pi$ ground state of HC_2I^+ is limited to that contained in the He I photoelectron spectrum[1–3] which reveals a strong band located 0.40(1) eV ($\sim 3230(80)$ cm^{-1}) above the origin of the $X^+\ ^2\Pi_{3/2} \leftarrow\ ^1\Sigma^+$ transition. In the same spectral region, one also expects to observe a band corresponding to the $X^+\ ^2\Pi_{3/2}(1^1)$

state of HC_2I^+. Indeed, Fulara *et al.*[6] have observed a band in the electronic spectrum of HC_2I^+ located 3258 cm^{-1} above the $^2\Pi_{3/2}$ origin which they attributed to a transition to the $^2\Pi_{3/2}(1^1)$ level. Thus at least two bands may contribute to the He I photoelectron spectra in the vicinity of the upper $^2\Pi_{1/2}$ component. To clarify the spectral assignments and obtain a precise value of the spin-orbit splitting of the $^2\Pi$ ground state of HC_2I^+, the PFI-ZEKE photoelectron spectrum of HC_2I was recorded in the vicinity of the expected position of the (0_0^0, $\Omega = 1/2$) band. The experimental spectrum, displayed in Fig. 5, consists of two main features, a strong one centered at a wavenumber of 81553 cm^{-1}, and a weaker one centered at 81595 cm^{-1}. A third very weak band, designated by an asterisk in Fig. 5 was also observed in this region, but its intensity was found to be dependent on the experimental conditions (e.g., nozzle stagnation pressure and Ar:HC_2I mixing ratio), which strongly suggests that it is either a sequence band or a band of Ar-HC_2I.

We attribute the stronger band to the (0_0^0, $\Omega = 1/2$) band and the weaker one to the (1_0^1, $\Omega = 3/2$) band, primarily on the basis of expected Franck-Condon factors for the excitation of the C-H stretching vibration. Indeed, we do not expect the $X^+ \leftarrow X$ ionization to significantly affect the C-H bond so that the 0_0^0 bands should be stronger than the 1_0^1 bands. This assignment is indirectly supported by the intensity distribution of the He I photoelectron spectrum of Allan *et al.*[3] Indeed, assigning the strong band observed at 10.1 eV in this spectrum to the (1_0^1, $\Omega = 3/2$) band would imply that a (1_0^2, $\Omega = 3/2$) band should also be observable in the He I photoelectron spectrum at a position of $\sim$ 10.5 eV, in contrast to the observation. One must therefore conclude that the (1_0^1, $\Omega = 3/2$) band is weaker than the (0_0^0, $\Omega = 1/2$) band, as is the case for our proposed assignment of the spectrum displayed in Fig. 5. Consequently, the spin-orbit splitting $\Delta\tilde{\nu}_{SO}$ of the $^2\Pi$ ground state of HC_2I^+ is 3257(1) cm^{-1} and the fundamental wavenumber of the C-H stretching vibration of HC_2I^+ is 3298(1) cm^{-1}. Fulara *et al.* have reported a value of 3258 cm^{-1} for the C-H stretching fundamental wavenumber but also suggested that the weak bands involving the upper $^2\Pi_{1/2}$ spin-orbit component are observable in their spectrum.

The value of 3257(1) cm^{-1} obtained for the spin-orbit splitting of the X^+ $^2\Pi$ ground state of HC_2I^+ is clearly large enough to justify the treatment of the (5_0^1, $\Omega = 3/2$) band in the limiting

case $|A_{\rm eff}| \gg (\omega_4,\ \omega_5)$ of the Renner-Teller effect.

Discussion and conclusions

The analysis of the Renner-Teller effect and spin-orbit coupling in $^2\Pi$ states of triatomic and tetraatomic molecules using expressions derived in earlier studies[8,10–12,14,22,32] has enabled the distinction of limiting cases characterized by the relative magnitude of the spin-orbit-coupling constant and bending frequencies. When the spin-orbit-coupling constant is much larger than the harmonic frequencies of the Renner-Teller active modes, the Renner-Teller effect is entirely masked and the $^2\Sigma_{1/2}$ and $^2\Delta_{5/2}$ components of the fundamental bands of these modes become almost degenerate. A residual splitting in the limit $|A| \to \infty$ results from vibronic interaction with electronic state of $^2\Sigma$ and $^2\Delta$ symmetry. When the spin-orbit-coupling constant is much smaller than the harmonic frequencies, the Renner-Teller effect leads to a reduction of the spin-orbit splittings, which can be expressed by analytical formulae (see Eq. (12)). When the spin-orbit-coupling constant is comparable to the vibrational frequencies strong perturbations of the energy level structure can arise whenever $|A_{\rm eff}| = 2\omega_{\rm b}$ for triatomic molecules, and $|A_{\rm eff}| = 2\omega_5$, $|A_{\rm eff}| = 2\omega_4$ and $|A_{\rm eff}| = \omega_5 + \omega_4$ in tetraatomic molecules.

The measurement and analysis of the partially rotationally resolved PFI-ZEKE photoelectron spectra of HC_2I has provided new spectroscopic informations on the $X^+\ ^2\Pi$ ground state of HC_2I^+. HC_2I^+ is confirmed to be a linear molecule in its $X^+\ ^2\Pi$ ground state. The ground electronic state $X^+\ ^2\Pi$ of HC_2I^+ corresponds to the first limiting case for which $|A_{\rm eff}| \gg (\omega_4,\ \omega_5)$. The large spin-orbit interaction leads to a splitting of 3257(1) cm^{-1} between the $^2\Pi_{3/2}$ lower and $^2\Pi_{1/2}$ upper spin-orbit components, and almost entirely quenches the Renner-Teller effect, which is only detectable, at low energies, through the observation of the forbidden 5_0^1 band. The two ($^2\Sigma_{1/2}$ and $^2\Delta_{5/2}$) vibronic components of the 5_0^1 level are almost degenerate, and their splitting of ~ 2 cm^{-1} is attributed to a vibronic interaction with excited electronic states of $^2\Sigma^+$ symmetry.

The vibronic energy structure and molecular constants of the HC_2I^+ ground state derived from

our PFI-ZEKE photoelectron spectra are summarized in Table 1. These results are compatible with earlier results derived from He I photoelectron spectra and optical spectra.[1,3,6] Though large (3257 cm^{-1}), the spin-orbit splitting in the X $^2\Pi$ ground state is significantly smaller than in HI^+ ($|A| = 5404$ cm^{-1} [33]) and CH_3I^+ ($|A| = 5053$ cm^{-1} [34]) where it corresponds closely to the I atomic value ($a = \frac{2}{3}(E(I\,^2P_{1/2}) - E(I\,^2P_{3/2})) = 5069$ cm^{-1} [35]). In the case of CH_3I^+, the atomic-like value of the spin-orbit-coupling constant was interpreted as being indicative of an almost complete localization of the positive charge on the I atom ($p_{x,y}$ electron hole), and was accounted for quantitatively in the realm of two-state charge-transfer model for cations of the family CH_3X^+ (X=F, Cl, Br and I).[36]

Applying the same model to cations of the HC_2X^+ family, the adiabatic ionization energies and spin-orbit splittings can be derived from the 2×2 matrix

$$H_{exc} = \begin{pmatrix} E_I(X) & V_X \\ V_X & E_I(HC_2H) \end{pmatrix} \tag{17}$$

where $E_I(X)$ is the center of gravity of the $^2P_{3/2}$ and $^2P_{1/2}$ ionization thresholds of the halogen atom, $E_I(HC_2H)$ is the vertical ionization threshold of acetylene (HC_2H) and V_X is the interaction potential. The eigenvalues of the matrix give the energetic positions of the $X^+\,^2\Pi$ ground state (E_-) and the $A^+\,^2\Pi$ first excited state (E_+) of the HC_2X^+ cation with respect to the $X\,^1\Sigma^+$ ground state of the neutral molecule. The corresponding eigenfunctions are

$$\phi_- = c_X \cdot \phi_X - c_{HC_2H} \cdot \phi_{HC_2H} \tag{18}$$

$$\phi_+ = c_X \cdot \phi_X + c_{HC_2H} \cdot \phi_{HC_2H} \tag{19}$$

with $c_X^2 + c_{HC_2H}^2 = 1$. The two parameters (c_X^2 and $c_{HC_2H}^2$) determine the iodine and CC-triple-bond character of the electron hole in the HC_2I^+ cation, respectively. The spin-orbit-coupling constant can be expressed as $c_X^2 \cdot a_X$, with a_X being the atomic spin-orbit-coupling constant of the halogen atom X.

The values of V_X were determined by comparing the eigenvalues of Eq. (17) with the vertical ionization energies of the $X^+\,^2\Pi \leftarrow X\,^1\Sigma^+$ and $A^+\,^2\Pi \leftarrow X\,^1\Sigma^+$ transitions of HC_2X (X= F, Cl, Br and I), determined as the center of gravity of the spin-orbit components in the photoelectron spectra[1,3] in a procedure illustrated in Fig. 6. In this figure, the two eigenvalues of Eq. (17) calculated with the known values of $E_I(X)$ [37–39] and $E_I(HC_2H)$ [40] are plotted as a function of V_X.

The optimal values of V_X correspond to the values at which the eigenvalues of Eq. (17) match the positions of the vertical ionization energies of the $X^+ \leftarrow X$ and $A^+ \leftarrow X$ bands. The input data used for this analysis and its results are summarized in Table 2. For HC_2I^+, the results imply that 29% of the positive charge is transferred to the $C \equiv C - H$ part of the molecule and that, consequently, the spin-orbit-coupling constant in the X^+ ground state should be only 71% of the atomic value, i.e., 3599 cm^{-1}. The reduction of the spin-orbit-coupling constant in HC_2I^+ from its atomic value is therefore not caused by the Renner-Teller effect but by charge transfer. In this simple model, the orbital hole can be regarded as being of mixed $p_{x,y}$ (I) and $C \equiv C$ π orbital character, which in turn provides explanations for the increase in the rotational constant upon ionization and for the many rotational branches observed in the photoelectron spectrum.

While extending the two-state charge-transfer model we had used to account for the spin-orbit splittings in the X ^{2}E ground state of the CH_3I^+ cations to HC_2I^+ cation, we noticed that our procedure is similar in spirit to the model called ZDO-MO used by Haink *et al.* to account for the main features of the He I photoelectron spectrum of HC_2X molecules.[1]

The behavior observed in HC_2X^+ and CH_3X^+ (X= F, Cl, Br and I) suggest that the spin-orbit splittings observed in the ground electronic states of radical cations of the type RX^+ are a direct measure of the extent of charge transfer between the halogen and the hydrocarbon rest R.

Acknowledgement

This work was supported financially by the Swiss National Science Foundation under project Nr. 200020-135342.

Supporting Information Available

The description of the iodoacetylene synthesis is given in the Supporting Information. This material is available free of charge via the Internet at `http://pubs.acs.org/`.

References

(1) Haink, H. J.; Heilbronner, E.; Hornung, V.; Kloster-Jensen, E. *Helv. Chim. Acta* **1970**, *53*, 1073–1083.

(2) Manne, R.; Wittel, K.; Mohanty, B. S. *Mol. Phys.* **1975**, *29*, 485–500.

(3) Allan, M.; Kloster-Jensen, E.; Maier, J. P. *J. Chem. Soc., Faraday Trans. 2* **1977**, *73*, 1406–1416.

(4) Maier, J. P.; Ochsner, M. *J. Chem. Soc., Faraday Trans. 2* **1985**, *81*, 1587–1598.

(5) Maier, J. P. *Phil. Trans. R. Soc. London Ser. A* **1988**, *324*, 209–221.

(6) Fulara, J.; Klapstein, D.; Kuhn, R.; Maier, J. P. *J. Phys. Chem.* **1986**, *90*, 2061–2067.

(7) Herzberg, G. *Molecular Spectra and Molecular Structure, Volume III, Electronic Spectra and Electronic Structure of Polyatomic Molecules*, 2nd ed.; Krieger Publishing Company: Malabar, 1991.

(8) Hougen, J. T. *J. Chem. Phys.* **1962**, *36*, 519–534.

(9) Brown, J. M. *J. Mol. Spectrosc.* **1977**, *68*, 412–422.

(10) Gauyacq, D.; Jungen, C. *Mol. Phys.* **1980**, *41*, 383–407.

(11) Sears, T. J. *Mol. Phys.* **1986**, *59*, 259–274.

(12) Tang, J.; Saito, S. *J. Chem. Phys.* **1996**, *105*, 8020–8033.

(13) Perić, M.; Peyerimhoff, S. D. *J. Mol. Spectrosc.* **2002**, *212*, 153–161.

(14) He, S. G.; Clouthier, D. J. *J. Chem. Phys.* **2005**, *123*, 014316.

(15) Hoshina, K.; Endo, Y. *J. Chem. Phys.* **2007**, *127*, 184304.

(16) Hollenstein, U.; Seiler, R.; Schmutz, H.; Andrist, M.; Merkt, F. *J. Chem. Phys.* **2001**, *115*, 5461–5469.

(17) Hollenstein, U.; Palm, H.; Merkt, F. *Rev. Sci. Instrum.* **2000**, *71*, 4023–4028.

(18) Rupper, P.; Merkt, F. *Rev. Sci. Instrum.* **2004**, *75*, 613–622.

(19) Jenkner, H. Verfahren zur Herstellung von Zinnaethinylen. CAPLUS AN 1964:3277(Patent) DE1152106 (B), 1963.

(20) Ku, Y.-Y.; Grieme, T.; Sharma, P.; Pu, Y.-M.; Raje, P.; Morton, H.; King, S. *Org. Lett.* **2001**, *3*, 4185–4187.

(21) Reiser, G.; Habenicht, W.; Müller-Dethlefs, K.; Schlag, E. W. *Chem. Phys. Lett.* **1988**, *152*, 119–123.

(22) Pople, J. A. *Mol. Phys.* **1960**, *3*, 16–22.

(23) Northrup, F.; Sears, T. J. *Mol. Phys.* **1990**, *71*, 45–64.

(24) Sommavilla, M.; Merkt, F. *J. Phys. Chem. A* **2004**, *108*, 9970–9978.

(25) He, S.-G.; Li, H.; Smith, T. C.; Clouthier, D. J.; Merer, A. J. *J. Chem. Phys.* **2003**, *119*, 10115–10124.

(26) Mishra, S.; Domcke, W.; Poluyanov, L. V. *Chem. Phys.* **2006**, *327*, 457–467.

(27) Zehnder, O.; Mastalerz, R.; Reiher, M.; Merkt, F.; Dressler, R. A. *J. Chem. Phys.* **2008**, *128*, 234306.

(28) Fulara, J.; Klapstein, D.; Kuhn, R.; Maier, J. P. *J. Phys. Chem.* **1985**, *89*, 4213–4219.

(29) Ahonen, A. M.; Ahonen, T.; Alanko, S. *J. Mol. Spectrosc.* **1998**, *191*, 117–124.

(30) Xie, J.; Zare, R. N. *The J. Chem. Phys.* **1992**, *97*, 2891–2899.

(31) Merkt, F.; Softley, T. P. *Int. Rev. Phys. Chem.* **1993**, *12*, 205–239.

(32) Yoshikawa, T.; Sumiyoshi, Y.; Takada, H.; Hoshina, K.; Endo, Y. *J. Chem. Phys.* **2008**, *128*, 204308.

(33) Potts, A. W.; Price, W. C. *Trans. Farad. Soc.* **1971**, *67*, 1242–1252.

(34) Grütter, M.; Michaud, J. M.; Merkt, F. *J. Chem. Phys.* **2011**, *134*, 054308.

(35) Sansonetti, J. E.; Martin, W. C.; Young, S. L. Handbook of Basic Atomic Spectroscopic Data (version 1.1.2). [Online] http://physics.nist.gov/Handbook [2010, Nov 18], 2005.

(36) Grütter, M.; Qian, X.; Merkt, F. *J. Chem. Phys.* **2012**, *137*, 084313.

(37) Moore, C. E. *Atomic Energy Levels*; NBS Circular 467/1; National Bureau of Standards: Washington, D. C., 1949.

(38) Moore, C. E. *Atomic Energy Levels*; NBS Circular 467/2; National Bureau of Standards: Washington, D. C., 1952.

(39) Moore, C. E. *Atomic Energy Levels*; NBS Circular 467/3; National Bureau of Standards: Washington, D.C., 1958.

(40) Kimura, K.; Katsumata, S.; Achiba, Y.; Yamazaki, T.; Iwata, S. *Handbook of HeI photoelectron spectra of fundamental organic molecules : ionization energies, ab initio assignments, and valence electronic structure for 200 molecules*; Japan scientific Societies Press: Tokyo, 1981.

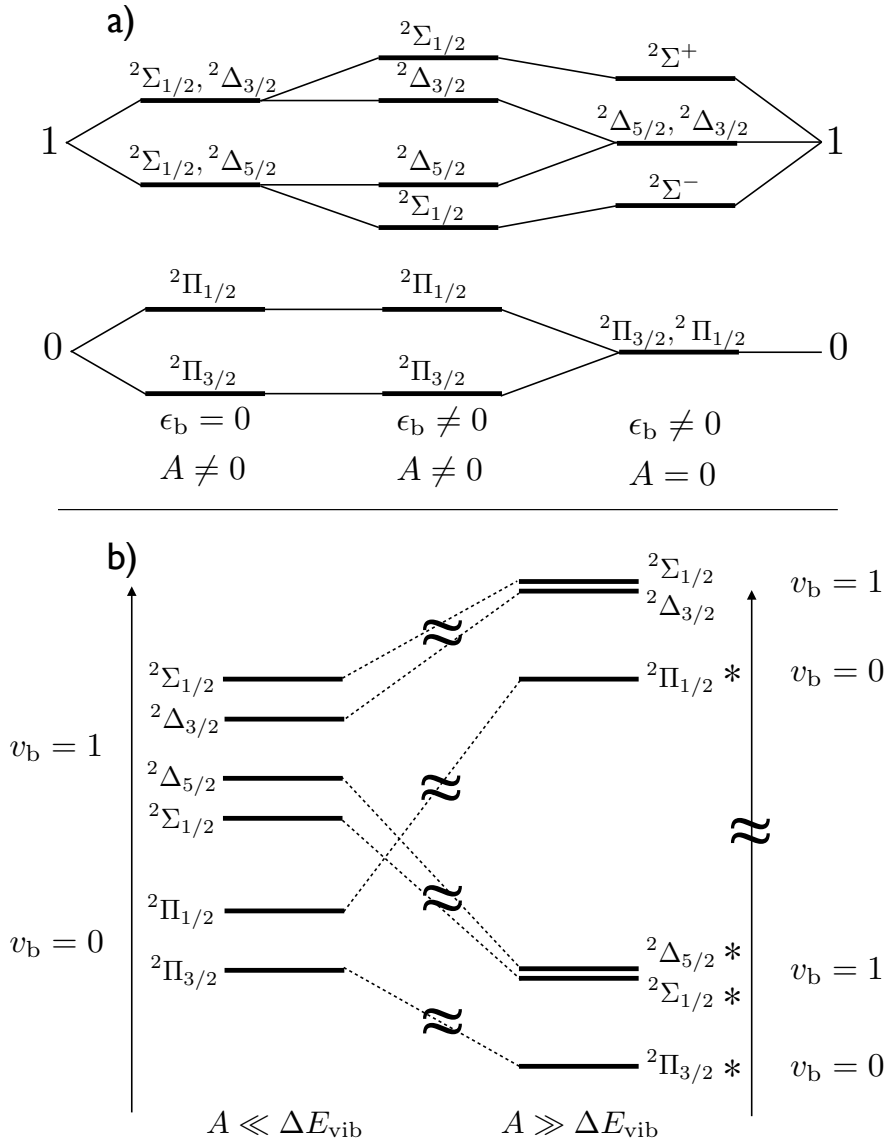

Figure 1: Energy level structure of a triatomic molecule in a $^2\Pi$ electronic state subject to the Renner-Teller effect. Panel a): situation for $|A| \ll \omega_b$. Left: $\varepsilon_b = 0, A \neq 0$. Right: $\varepsilon_b \neq 0, A = 0$. Middle: $\varepsilon_b \neq 0, A \neq 0$. (adapted from Ref. 7). Panel b) Correlation diagram connecting the limiting cases $|A| \ll \omega_b$ (left) and $|A| \gg \omega_b$ (right).

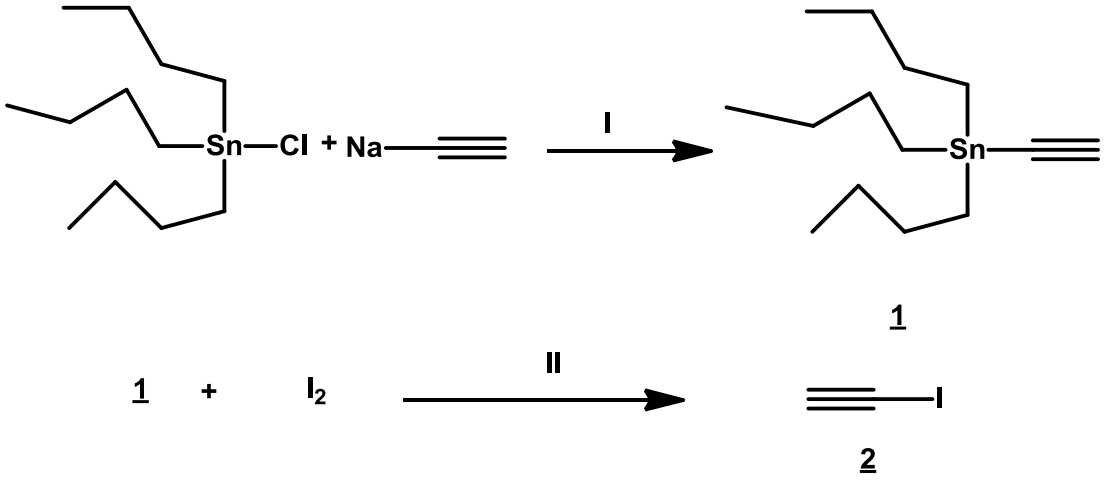

Scheme 1: Synthesis of iodoacetylene in two steps via tributyl(ethynyl)stannane (see also text and the Supporting Information).

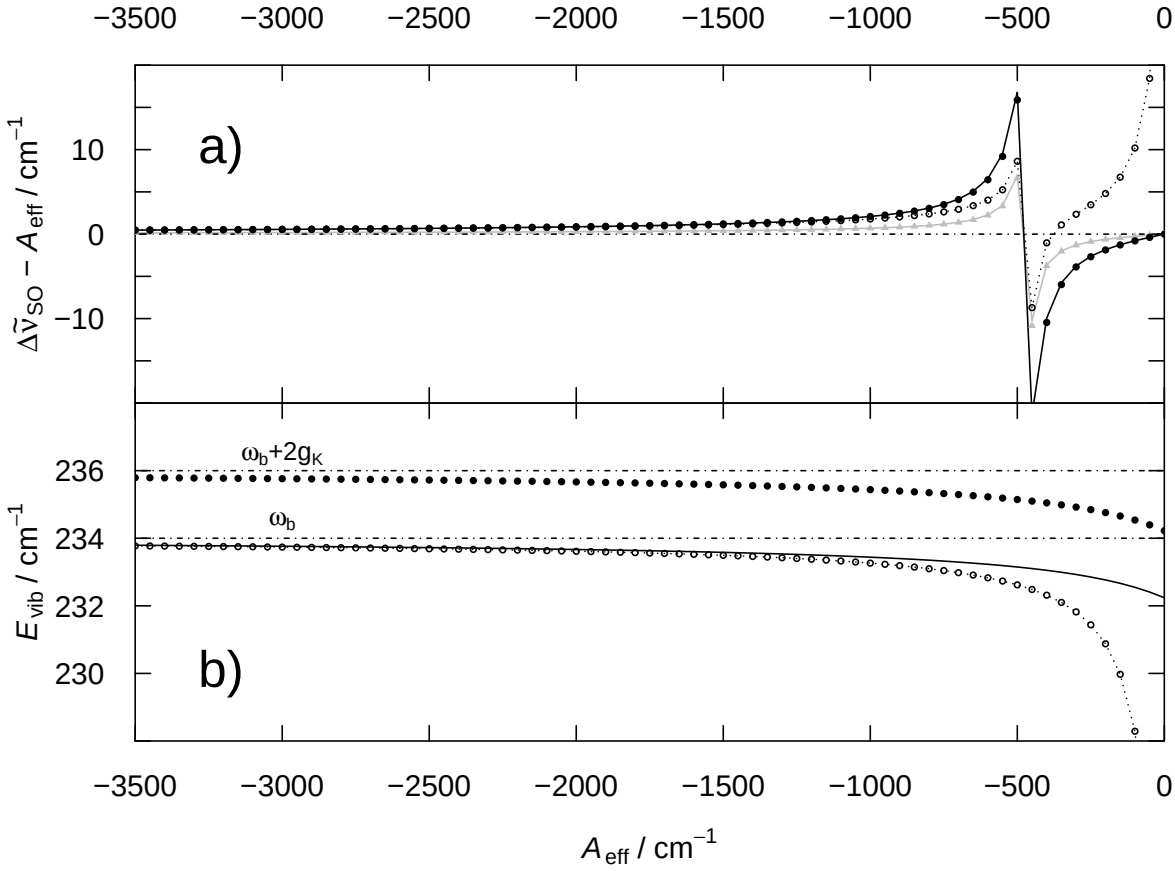

Figure 2: Calculated spin-vibronic energy level structure of a triatomic molecule with $\omega_b = 234$ cm^{-1}, $\varepsilon_b = 0.1$ and $g_K = 1$ cm^{-1}. Panel a) displays the differences between the calculated spin-orbit splitting $\Delta\tilde{\nu}_{SO}$ and the spin-orbit-coupling constant A_{eff} as a function of A_{eff} for a $^2\Pi$ ground state (grey triangles and line) and for the $^2\Sigma$ (open circles and dotted line) and $^2\Delta$ (full circles and line) components of the $v_b = 1$ level. Panel b) represents the $^2\Sigma_{1/2}$ (dotted line and open circles) and $^2\Delta_{5/2}$ (full line and circles) vibronic level energies with respect to the $^2\Pi_{3/2}$ ground state energy, obtained using Eqs. (3)-(7) (circles) and only Eqs. (3)-(6) (lines).

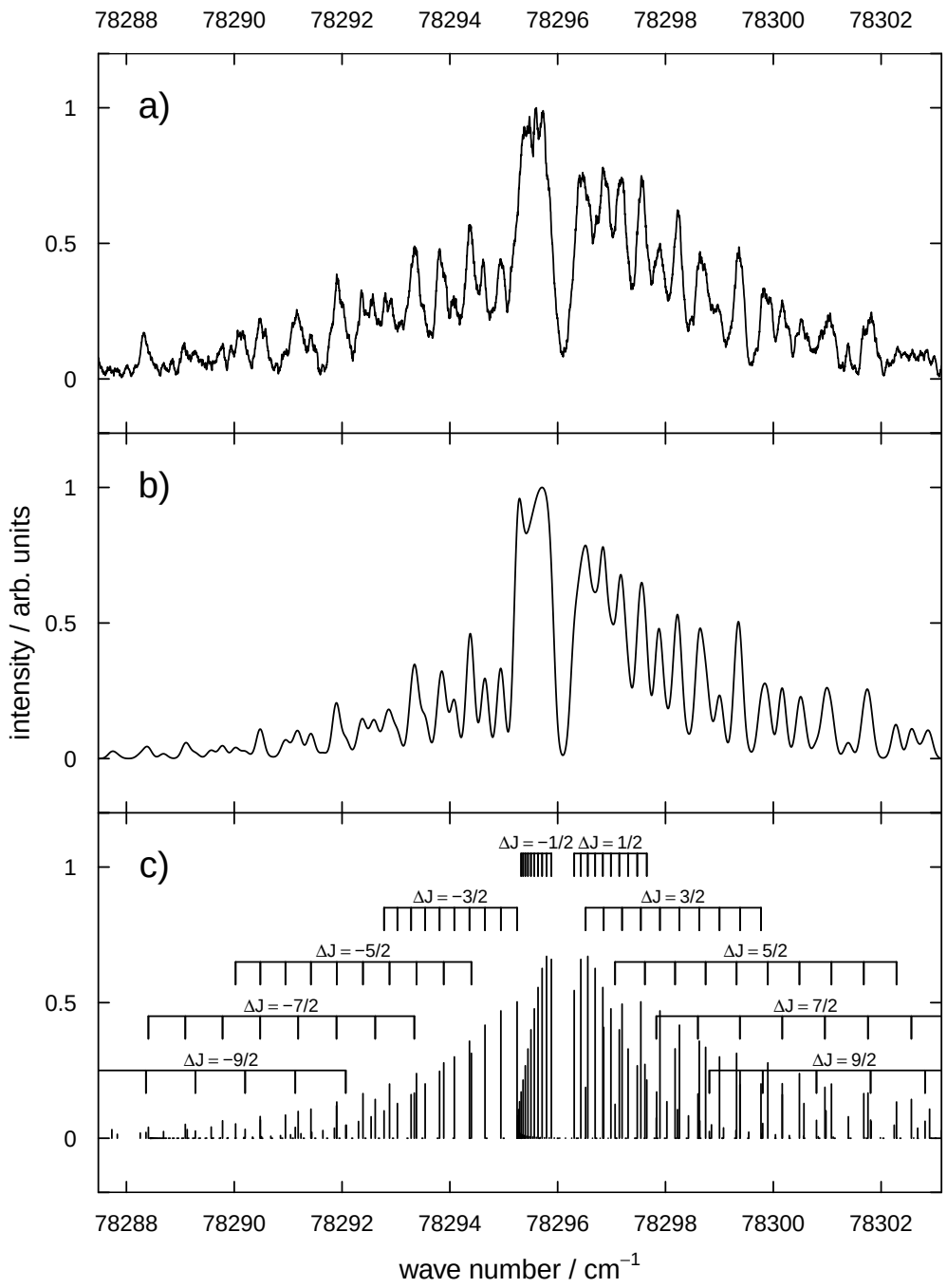

Figure 3: PFI-ZEKE photoelectron spectrum of the $X^+\ ^2\Pi_{3/2}(v=0) \leftarrow X\ ^1\Sigma^+(v=0)$ transition of HC_2I. The experimental spectrum (top panel) is compared with the calculated stick spectrum (bottom panel) and a spectrum obtained by its convolution with a Gaussian line-shape function (FWHM = 0.17 cm^{-1}) (middle panel).

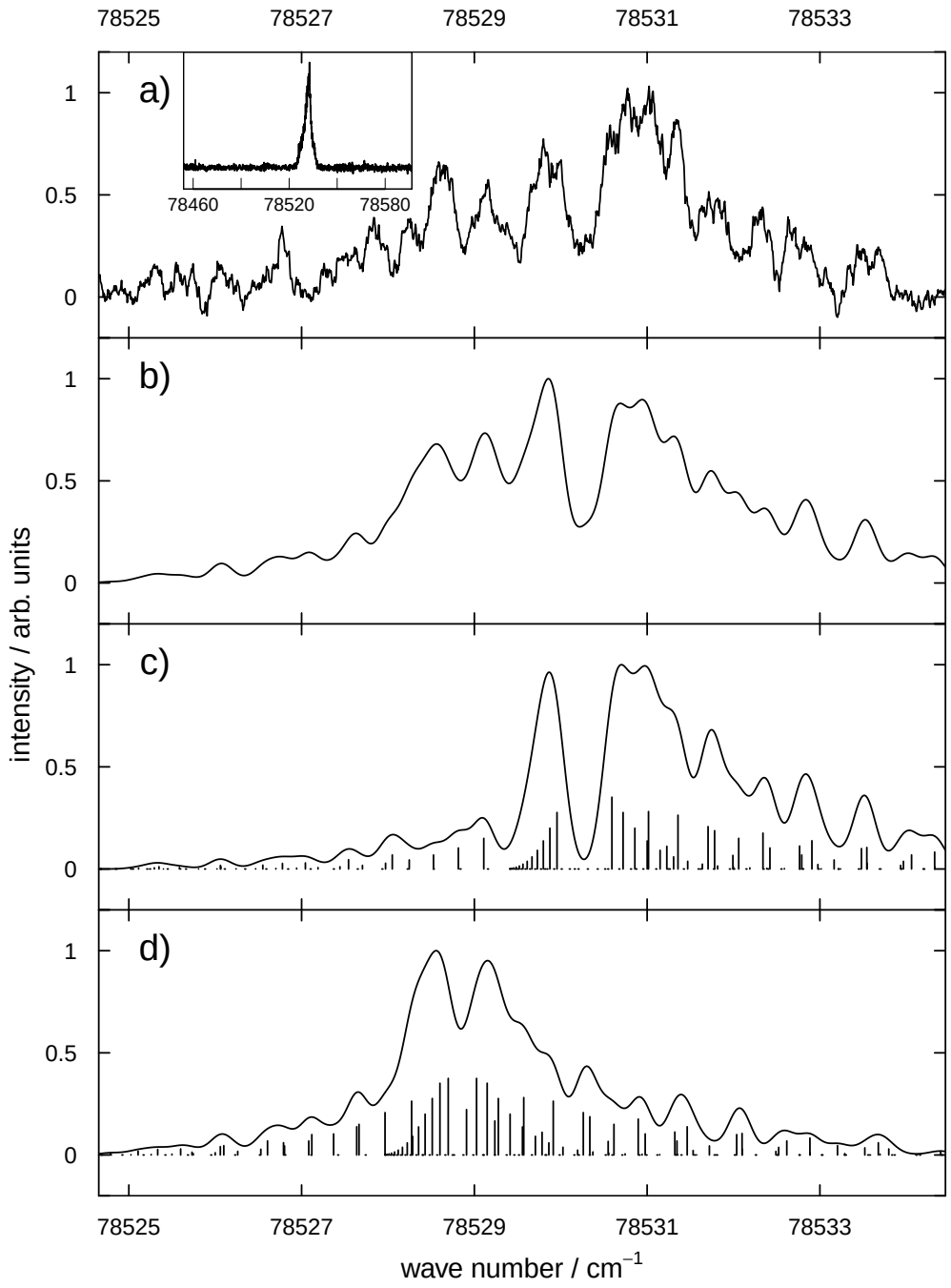

Figure 4: PFI-ZEKE photoelectron spectrum of the $X^+\ ^2\Pi_{3/2}(v_5 = 1) \leftarrow X\ ^1\Sigma^+(v = 0)$ transition of HC_2I. a) Experimental spectrum with an overview spectrum in the inset. b) Calculated spectrum obtained by adding the contributions of the $^2\Delta_{5/2}$ and $^2\Sigma_{1/2}$ bands. c) Calculated spectrum of the $^2\Delta_{5/2} \leftarrow^1 \Sigma^+$ band. d) Calculated spectrum of the $^2\Sigma_{1/2} \leftarrow^1 \Sigma^+$ band. The calculated spectra were obtained from the calculated stick spectra after convolution with a Gaussian line shape function with a full width at half maximum of 0.3 cm^{-1}.

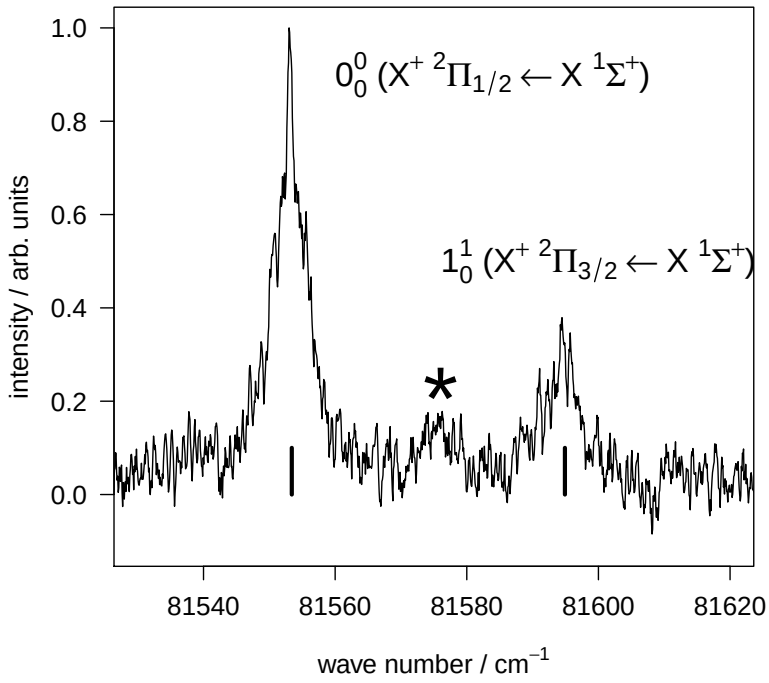

Figure 5: PFI-ZEKE photoelectron spectrum of HC_2I in the vicinity of the $X^+\ ^2\Pi_{1/2}(v=0) \leftarrow X\ ^1\Sigma^+(v=0)$ and the $X^+\ ^2\Pi_{3/2}(v_1=1) \leftarrow X\ ^1\Sigma^+(v=0)$ transitions. The full line corresponds to the experimental spectrum. The weak peak marked by an asterisk is attributed to a band of Ar-HC_2I. The origins of the bands obtained from an analysis of the rotational contours are indicated by vertical bars.

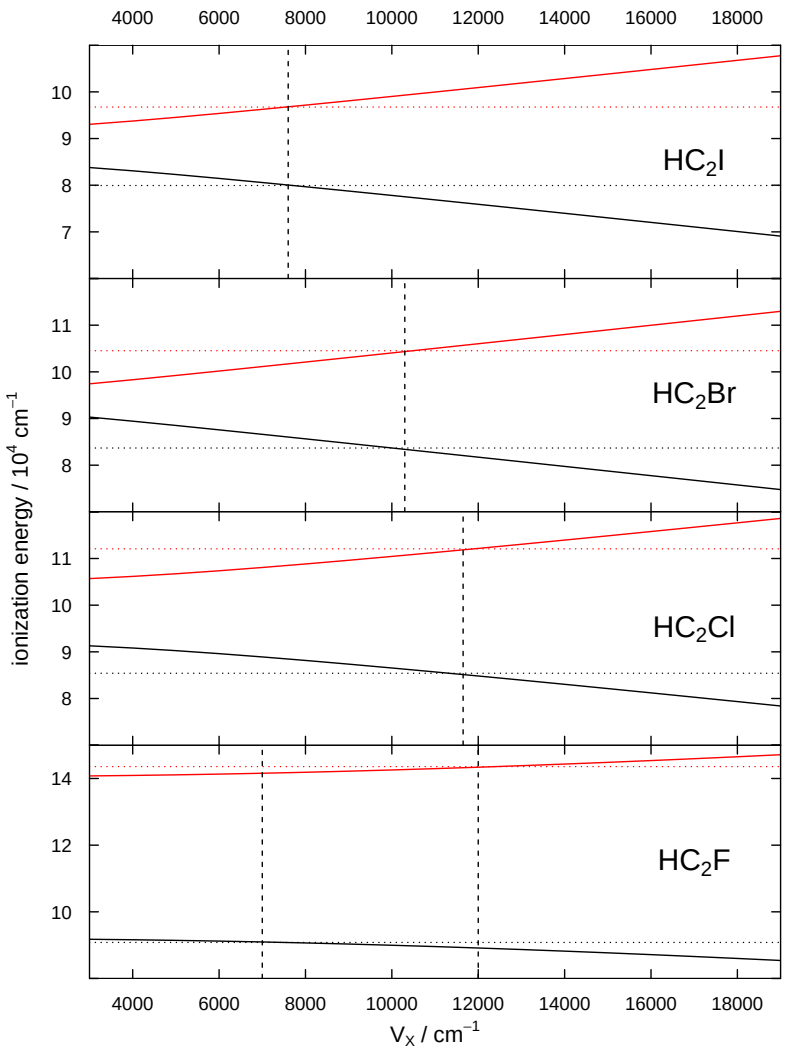

Figure 6: Calculated vertical ionization energies of the acetyl halides (HC_2X with X=F, Cl, Br or I) obtained with the two-state charge-transfer model as a function of the interaction potential V_X (solid lines). The horizontal dotted lines represent the experimental values from Refs. 1,3 and this work. The upper and lower lines represent the ionization energies to the $X^+\ ^2\Pi$ and the $A^+\ ^2\Pi$ states of the cations, respectively. The values of the interaction potential which give the best agreement between the experimental and the calculated ionization energies are marked by dashed vertical lines. In the case of HC_2F^+, the two dashed lines delimit the range of V_X values where a satisfactory agreement with experimental results can be reached.

Table 1: Molecular constants of the $X^+\ ^2\Pi$ ground state of HC_2I^+ determined in this work and comparison with previous results. All values are in cm^{-1}.

	this work	Refs. 4,6	Ref. 3	Ref. 1
$E_I(X^+\ ^2\Pi_{3/2}, v=0, J=\frac{3}{2})/(hc)$	78296.5(2)	-	78316(80)	78478(160)
$B_0^+(X^+\ ^2\Pi_{3/2}, v=0)$	0.1093(8)	0.10959(7)	-	-
$E_I(X^+\ ^2\Pi_{1/2}, v=0, J=\frac{1}{2})/(hc)$	81553(1)	-	81542(80)	81785(160)
$\Delta\tilde{\nu}_{SO}$ ($X^+\ ^2\Pi$, v=0)	3257(1)	-	3226(80)	3307(160)
$E_I(X^+\ ^2\Sigma_{1/2}, v_5=1, J=\frac{1}{2})/(hc)$	78528.9(5)	-	-	-
$E_I(X^+\ ^2\Delta_{5/2}, v_5=1, J=\frac{5}{2})/(hc)$	78531.3(5)	-	-	-
ω_5	234(1)	237(2)	-	-
$E_I(X^+\ ^2\Pi_{3/2}, v_1=1, J=\frac{3}{2})/(hc)$	81595(1)	-	-	-
ω_1	3298(1)	3258(2)	-	-

Table 2: Ionization energies ($E_{\mathbf{I}}/(hc)$ in $\mathbf{cm^{-1}}$) and spin-orbit splittings ($\Delta\tilde{\nu}_{\mathbf{SO}}$ in $\mathbf{cm^{-1}}$) corresponding to the lowest two $^2\Pi$ states of $\mathbf{HC_2X^+}$ (X=F, Cl, Br and I), and parameters ($E_{\mathbf{I,X}}/(hc)$, $E_{\mathbf{I,C_2H_2}}/(hc)$, $V_{\mathbf{X}}$ and $A_{\mathbf{X}}$, all in $\mathbf{cm^{-1}}$) used to calculate them using a two-state charge-transfer model.

	HC_2I	HC_2Br	HC_2Cl	HC_2F	Ref.
$E_{\mathrm{I,X}}/(hc)$	84886	95795	105040	140587	37–39
$E_{\mathrm{I},C_2H_2}/(hc)$	91953.5	91953.5	91953.5	91953.5	18
V_{X}	7600	10300	11650	[7000-12000]	
$E_{-}^{\mathrm{calc}}/(hc)$	80036	83393	85130	[90960-89148]	
$E_{+}^{\mathrm{calc}}/(hc)$	96796	104349	111857	[141574-143386]	
$E_{-}^{\mathrm{exp}}/(hc)$	79925[a]	83680	85414	90818	1,3
$E_{+}^{\mathrm{exp}}/(hc)$	96746	104529	112071	143567	1,3
c_{X}^2	0.71	0.41	0.26	[0.02-0.05]	
A_{X}	5069	2457	588	269	35
$\Delta\tilde{\nu}_{\mathrm{SO}}^{\mathrm{calc}} = c_{\mathrm{X}}^2 A_{\mathrm{X}}$	3599	1007	153	[5.38-13.45]	
$\Delta\tilde{\nu}_{\mathrm{SO}}^{\mathrm{exp}} = A_{\mathrm{X}^+\,\mathrm{HC_2X}}^{\mathrm{exp}}$	3257[a]	1049	161	0[b]	1,3

[a] Values determined in this work.

[b] In Ref. 1, the spin-orbit splitting could not be resolved.

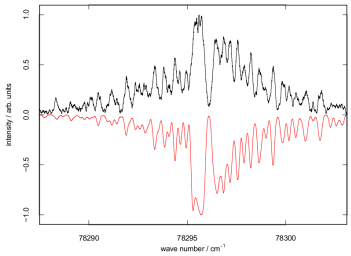

Figure 7: graphic for the TOC entry.